IEEE Photonics Journal
An IEEE Photonics Society Publication

UWB Monocycle Generation and Bi-Phase Modulation Based on Mach–Zehnder Modulator and Semiconductor Optical Amplifier

Volume 4, Number 2, April 2012

Yuan Yu
Jianji Dong
Xiang Li
Xinliang Zhang

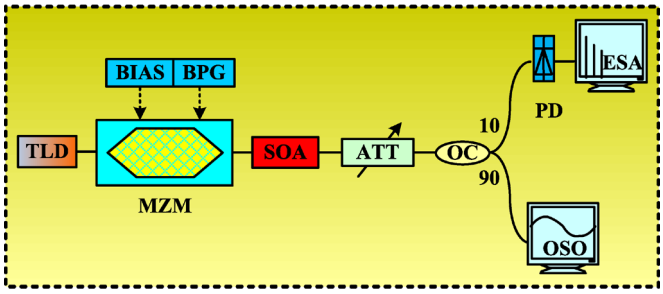

DOI: 10.1109/JPHOT.2011.2180014
1943-0655/$31.00 ©2012 IEEE

UWB Monocycle Generation and Bi-Phase Modulation Based on Mach–Zehnder Modulator and Semiconductor Optical Amplifier

Yuan Yu, Jianji Dong, Xiang Li, and Xinliang Zhang

Wuhan National Laboratory for Optoelectronics, School of Optoelectronic Science and Engineering, Huazhong University of Science and Technology, Wuhan 430074, China

DOI: 10.1109/JPHOT.2011.2180014
1943-0655/$31.00 ©2012 IEEE

Manuscript received September 1, 2011; revised December 6, 2011; accepted December 9, 2011. Date of publication December 15, 2011; date of current version February 28, 2012. This work was supported in part by the National Basic Research Program of China under Grant 2011CB301704 and the National Natural Science Foundation of China under Grant 60901006. Corresponding author: X. Zhang (e-mail: xlzhang@mail.hust.edu.cn).

Abstract: We propose and experimentally demonstrate an approach in generating a pair of polarity-reversed ultra-wideband (UWB) monocycle pulses by using a Mach–Zehnder modulator (MZM) and a semiconductor optical amplifier (SOA). The monocycle polarity is controlled by adjusting the bias voltage of the MZM to make the bias point located at the positive or the negative slope of the modulation curve. The generated UWB monocycles with different injection currents of SOA, different bias voltages of MZM, different optical pulse widths, and different optical carrier wavelengths are experimentally studied and analyzed. The bi-phase modulation (BPM) of monocycle pulse by applying nonreturn-to-zero (NRZ) data to the radio frequency (RF) port of MZM is also proposed and investigated.

Index Terms: Ultra-wideband (UWB), bi-phase modulation (BPM), Mach–Zehnder modulator (MZM), in-phase modulation, counter-phase modulation, semiconductor optical amplifier (SOA).

1. Introduction

Ultra-wideband (UWB) impulse radio is one of the most attractive techniques for short-range, high-capacity wireless communications due to its intrinsic advantages, such as immunity to multipath fading, being carrier free, broad bandwidth, and low-power spectral density (PSD) [1]–[3]. In 2002, the U.S. Federal Communications Commission (FCC) approved the 7.5-GHz spectral bandwidth from 3.1 GHz to 10.6 GHz for the unlicensed use of UWB for indoor communications. Based on the FCC definition, the UWB signal should have a 10-dB bandwidth of larger than 500 MHz (or a fractional bandwidth larger than 20%). Limited by the PSD of no more than -41.3 dBm/MHz [2], the UWB wireless distribution in free space is limited to only a few meters or tens of meters. UWB-over-fiber is an effective technology to increase the coverage of UWB signals by exploiting the advantages of optical fibers, and the UWB communication systems can be further integrated into optical networks [4], [5]. Thus, the generation, modulation, and distribution of UWB signals in the optical domain is strongly desired to avoid the extra cost of electrical–optical conversion [6]. A number of schemes have been proposed to generate UWB monocycle pulses. In addition to the simplicity and achievability, using Gaussian monocycle pulses in an UWB communication system can provide better bit error rate (BER) and multipath interference [6], [7]. Thus, many schemes achieving Gaussian monocycle

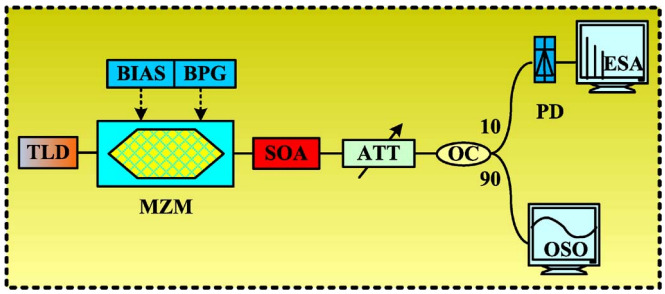

Fig. 1. Experimental setup.

pulses have been proposed and demonstrated [8]–[16]. According to the modulation format, these schemes can be generally classified into two categories: using phase modulation (PM) and PM to intensity modulation (IM) conversion, and using intensity modulation and superimposing optical pulses with opposite polarities. In the first category, the Gaussian pulse is phase modulated onto the optical carrier, and the UWB monocycle pulses are generated by using a frequency discriminator to realize PM–IM conversion [8]–[12]. In the second category, the Gaussian pulse is intensity modulated onto the optical carrier. By delaying and superimposing intensity pulses with opposite polarities, the UWB pulse is generated [13]–[15]. UWB modulation is another focus of UWB communication. However, most reported schemes can only implement on–off keying (OOK) modulation. The limitation of the OOK modulation of UWB is the low immunity to multipath effect, in which echoes of the original pulses make it difficult to determine the absence of a pulse. Additionally, OOK is a binary modulation format, which cannot be extended to an *M*-ary modulation [16]. However, bi-phase modulation (BPM) can overcome these limitations and has a signal-to-noise ratio (SNR) improvement of 3 dB. Thus, the UWB BPM has attracted great interest and different schemes have been proposed, such as using the relaxation oscillations of a distributed feedback (DFB) laser and incoherent summation of input optical signal and the output signal of a DFB laser [17], using a dual-drive Mach–Zehnder modulator (MZM) and an electrically reconfigurable asymmetric Mach–Zehnder interferometer (MZI) [18], and using PM–IM conversion and incoherently superimpose converted optical pulses to realize power-efficient UWB BPM [19].

In this paper, we propose and demonstrate a novel UWB impulse transmitter by using an MZM and a semiconductor optical amplifier (SOA). A pair of polarity-reversed monocycle pulses is generated by exploiting the nonlinear amplification process in SOA when the MZM is biased at opposite slopes. The negative monocycle pulse generation using the overshoot in SOA has been previously reported [20]. However, only negative monocycle pulse is achieved because the input optical signal of SOA is a fixed inverted return-to-zero (RZ) signal. Later, a UWB impulse generator based on the relaxation oscillations of a semiconductor laser is proposed and demonstrated [21]. In our scheme, the positive monocycle pulse generation using the undershoot, which is generated by injecting an optical RZ signal with a pedestal into the SOA, is proposed and experimentally demonstrated for the first time. Additionally, the BPM of monocycle pulse by switching the bias point of MZM is also proposed and investigated. In order to implement the BPM of monocycle pulse using a commercial MZM, we propose that the electrical signal is applied to the radio frequency (RF) port of the MZM rather than the bias port. To the best of our knowledge, this is the first time to propose and investigate UWB BPM by electrically switching the bias point of MZM.

2. Experimental Setup and Operation Principle

The proposed experimental setup is shown in Fig. 1. A continuous wave (CW) light emitted from the tunable laser diode (TLD) is intensity modulated by the MZM. The "BIAS" in Fig. 2 is a voltage source applied to the bias port of MZM to control the bias point of MZM. The MZM has a half-wave voltage of less than 8 V at the bias port. The bit pattern generator (BPG) is used to generate an

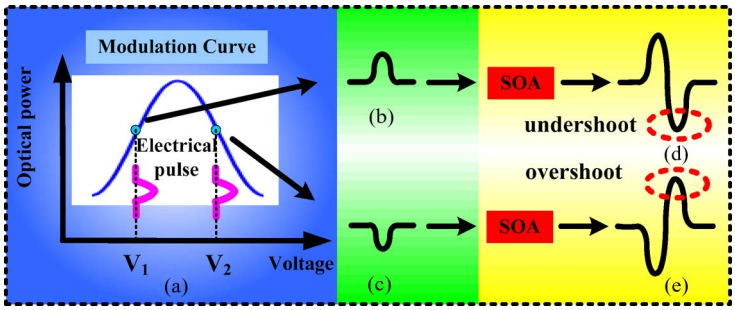

Fig. 2. Operation principle of the proposed scheme.

electrical RZ signal, which is injected into the RF port of MZM. Then, the intensity modulated optical signal is launched into the SOA. The SOA is a CIP nonlinear SOA, with a typical saturated gain recovery time $(1/e)$ of 16 ps. The ATT is used to protect the photodetector (PD) and the optical sampling oscillator (OSO) in the case of power damage. Then the optical signal is power split by a 10 : 90 optical coupler (OC). The 10% part is sent to the PD to be converted into the electrical signal. The RF spectrum is measured by the electrical spectrum analyzer (ESA). The other 90% part is sent to the OSO to display the waveform.

The operation principle is shown in Fig. 2. Fig. 2(a) shows the modulation curve of the MZM. The RF port of MZM is driven by an electrical RZ signal. When the bias voltage is V_1, the MZM operates at the positive slope of the modulation curve, and the modulated optical signal is in-phase with the electrical signal, as shown in Fig. 2(b). It should be noted that the optical signal is with a pedestal. Then the modulated optical signal is injected into the SOA. When the pedestal passes through the SOA, the carrier density stays at a higher level. When the positive Gaussian pulse passes through the SOA, the optical pulse gets amplified and the carrier density is decreased consequently. The lower carrier density leads to a smaller gain and an undershoot is formed just after the positive pulse. After the nonlinear amplification process, the carrier density gets recovered to the normal level and the optical pedestal at other duration time is uniformly amplified. Therefore, a positive monocycle pulse can be obtained, as shown in Fig. 2(d).

Oppositely, when the bias voltage is adjusted to V_2, the MZM operates at the negative slope of modulation curve, as shown in Fig. 2(a). Thus, the modulated optical signal is counter-phase with the electrical signal [22]. Therefore, a Gaussian pulse with inverted polarity is obtained, as shown in Fig. 2(c). At this time, when the inverted Gaussian pulse passes through the SOA, the optical power is lower than the optical direct current (DC) component, leading to an increase of carrier density. The higher carrier density leads to a larger gain in SOA and the optical DC component just after the negative Gaussian pulse gets over amplified and an optical overshoot is formed, as shown in Fig. 2(e). At other duration time, the optical power is also uniformly amplified. Therefore, a negative monocycle pulse is formed.

We can see that a pair of polarity-reversed monocycle pulses should be generated when the bias point of MZM is changed. If the bias point is electrically switched, the UWB BPM could be realized.

3. Experimental Results and Simulation Results About UWB BPM

The experiment is carried out based on the scheme shown in Fig. 1. The models and key parameters of equipment are list as follows: the emission power of LD (Agility 3205) is 10.6 dBm, the bit rate of BPG (SHF BPG 44E) is tunable and its maximum is 40 Gb/s, the frequency range of ESA (MS2668C) is from 0 to 40 GHz, and the bandwidth of OSO (Angilent Infiniium DCA-J 86100C) exceeds 80 GHz. In the experiment, the amplitude of the RZ signal that applied to the MZM is 0.95 V. The measured positive and negative monocycle pulses and their dependence on the bias current of SOA, bias voltage of MZM, bit rate of electrical signal, and carrier wavelength are presented in Sections 3.1 and 3.2, respectively. Discussions and simulations about the BPM of monocycle pulse are presented in Section 3.3.

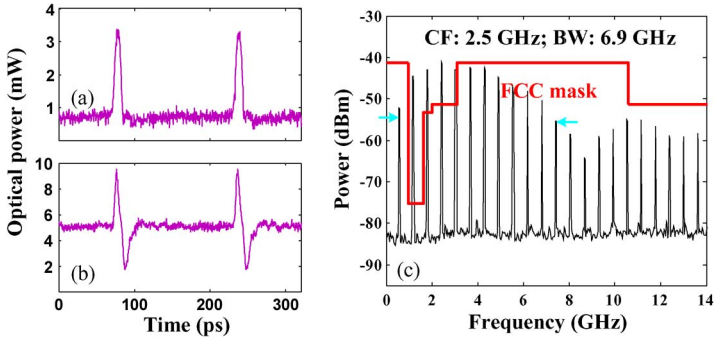

Fig. 3. (a) Intensity modulated optical pulse, (b) the generated optical waveform after SOA, and (c) its corresponding ESA.

3.1. Positive Monocycle Pulse Generation and Investigation

At first, the optical wavelength is set at 1549.88 nm. The bit sequence launched from BPG is set with a fixed pattern "1000 0000 0000 0000" (one "1" per 16 bits) at a bit rate of 10 Gb/s, indicating that the repetition rate is 625 MHz and the full-width at half-maximum (FWHM) is 50 ps. The MZM is biased at −3.93 V and operates at the positive slope of the modulation curve. The SOA is biased at 180 mA. The measured optical waveforms and its RF spectrum are shown in Fig. 3.

The optical waveform after the MZM is shown in Fig. 3(a). We can see that a RZ signal with a pedestal is generated. The maximal and the minimal optical power are 3.3 mW and 0.7 mW, respectively. When the optical signal is injected into the SOA, the measured optical waveform at the output of SOA is shown in Fig. 3(b). We can observe that a positive monocycle pulse is successfully generated. The upper and the lower amplitudes are 4.4 mW and 3.4 mW, and the upper and the lower FWHMs are 51 ps and 70 ps, respectively. Its RF spectrum is shown in Fig. 3(c). The center frequency [CF in Fig. 3(c)] and the 10-dB bandwidth [BW in Fig. 3(c)] are 2.5 GHz and 6.9 GHz (from 0.6 GHz to 7.5 GHz), respectively, with a fractional bandwidth of 276%. In Fig. 3(c), we can see that the RF power can be reduced low enough to meet the FCC requirement (no more than −41.3 dBm/MHz). However, the mask infringement can be observed in Fig. 3(c), especially at the global positioning system (GPS) band. This will limit the maximal emission power in practice. The RF power at the GPS band can be reduced with the help of the UWB antenna, which acts as a bandpass filter [16].

The bias current of SOA can affect the carrier density of SOA, thus affecting the generated monocycle pulses. Fig. 4 shows the generated optical pulses when the SOA is biased at different currents.

Fig. 4(a)–(c) show the measured optical waveforms when the SOA is biased at 120 mA, 180 mA and 240 mA, respectively. When the bias current is 120 mA, the upper and the lower amplitudes are 3.2 mW and 1.3 mW, and the upper and the lower FWHMs are 63 ps and 186 ps, respectively. Thus both the amplitude and the FWHM of the monocycle pulse show distinct asymmetry. When the bias current is increased to 180 mA, the upper and the lower amplitudes are 3.7 mW and 2.8 mW, and the upper and the lower FWHMs are 52 ps and 73 ps, respectively, with an improved symmetry. When the bias current is further increased to 240 mA, the upper and the lower amplitudes are 4.1 mW and 3.3 mW and the upper and the lower FWHMs are 48 ps and 66 ps, respectively. We can see that a larger bias current can improve the symmetry of the positive monocycle pulse. As the bias current is increased, both the center frequency and the 10-dB bandwidth do not show distinct variation, but the PSD at low frequencies is suppressed lower, which can be observed by comparing Fig. 4(d)–(f). Thus, a large bias current is preferred to improve the symmetry of positive monocycle pulse.

The bias voltage of MZM can also affect the generated positive monocycle pulses. We have a study about the influence of the bias voltage of MZM on the positive monocycle pulse. The bias current of SOA is set at 180 mA. The generated positive monocycle pulses and their RF spectra when the MZM is biased at −5.75 V, −3.93 V, and −2.66 V are shown in Fig. 5.

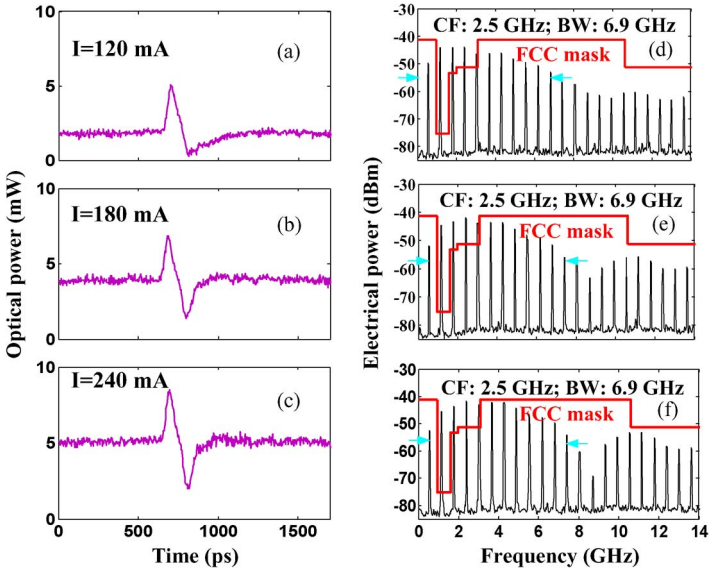

Fig. 4. (a)–(c) Generated positive monocycle pulses and (e)–(f) their corresponding RF spectra when the SOA is biased at 120 mA, 180 mA, and 240 mA.

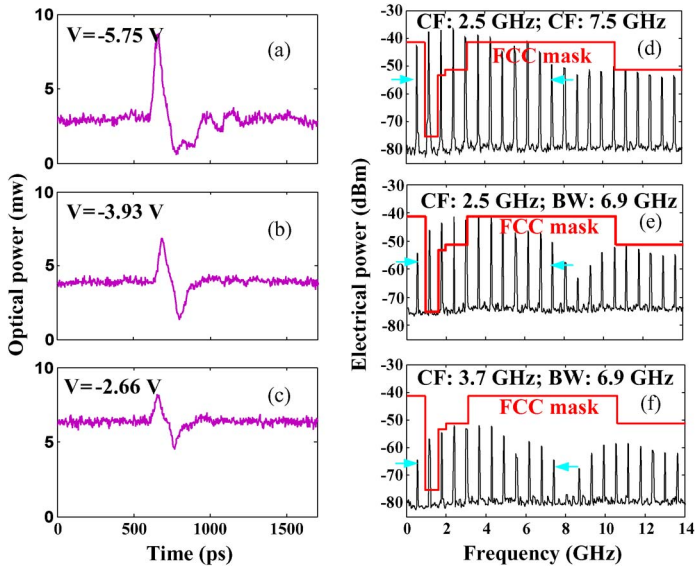

Fig. 5. (a)–(c) Generated monocycle pulses and (d)–(f) their corresponding RF spectra when the MZM is biased at −2.66 V, −4.51 V, and −5.75 V.

The generated positive monocycle pulse shows distinct asymmetry when the MZM is biased at −5.75 V, as shown in Fig. 5(a). The upper and the lower amplitudes are 5.7 mW and 2.1 mW, and the upper and the lower FWHMs are 55 ps and 174 ps, respectively. Therefore, the asymmetry monocycle pulse leads to a larger PSD at the low frequency, as shown in Fig. 5(d). When the bias voltage is increased to −3.93 V, the upper amplitude is decreased and the lower amplitude is increased, with an improved symmetry. When the bias current is further increased to −2.66 V, the upper and the lower amplitudes are 1.37 mW and 1.16 mW, and the upper and the lower FWHMs are 33 ps and 37 ps, respectively, as shown in Fig. 5(c). We can see that when the bias voltage is increased, the symmetry of the positive monocycle pulse is improved, but the PSD is decreased, and a peak-power reduction of 12 dB can be observed by comparing Fig. 5(e) and (f). Thus, a

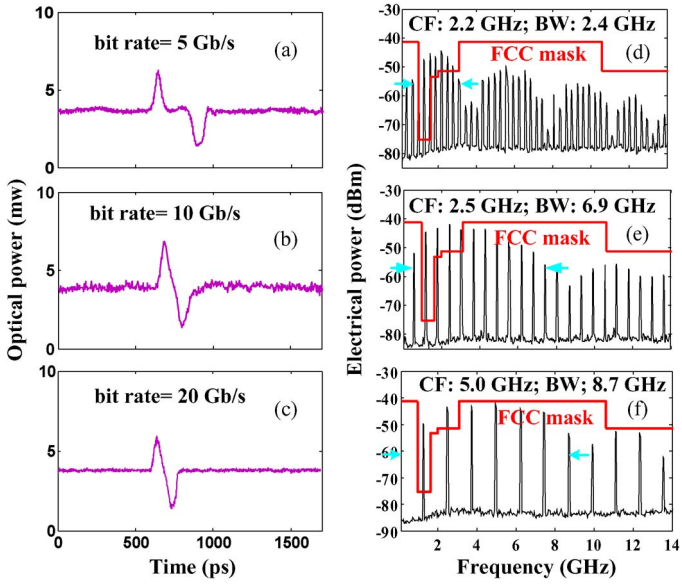

Fig. 6. Generated optical waveform when the FWHM is (a) 100 ps, (b) 50 ps, and (c) 25 ps and (d)–(f) their corresponding RF spectra, respectively.

balanced voltage is −3.93 V. The generated positive monocycle pulse and its RF spectrum are shown in Fig. 5(b) and (e), respectively.

Then, we change the bit rate of electrical RZ signal by tuning the BPG to change the pulse width. The measured optical pulses and the RF spectra when the bit rate of electrical signal is 5 Gb/s, 10 Gb/s, and 20 Gb/s are shown in Fig. 6 (the bit pattern is still fixed with one "1" per 16 bits). In Fig. 6(a), we can see that when the bit rate is 5 Gb/s, the lower part of generated optical pulse has a certain time delay compared with the upper part, and the optical pulse is not a UWB monocycle pulse. This is because when the bit rate is low, the electrical pulse generated by BPG is super-Gaussian like. When the optical super-Gaussian pulse is launched into the SOA, overshoot and undershoot can be formed at the rising edge and the trailing edge of the super-Gaussian pulse. Thus, a time delay between the overshoot and the undershoot can be observed. The center frequency and 10-dB bandwidth are 2.2 GHz and 2.4 GHz, respectively, as shown in Fig. 6(d). When the bit rate is 10 Gb/s, the generated monocycle pulse is shown in Fig. 6(b). Its RF spectrum is shown in Fig. 6(e). The center frequency and the 10-dB bandwidth are 2.5 GHz and 6.9 GHz, respectively. When the bit rate is increased to 20 Gb/s, the generated monocycle pulse is shown in Fig. 6(c) and its RF spectrum is shown in Fig. 6(f). The center frequency and the 10-dB bandwidth are 5.0 GHz and 8.7 GHz, respectively. The increasing bit rate of electrical signal leads to a decreasing of the electrical signal pulse width. Thus, the center frequency and 10-dB bandwidth are increased.

The influence of the optical carrier wavelength on the generated positive monocycle pulse is also studied. The measured center frequency and the 10-dB bandwidth when the optical wavelength is tuned in the C-band are shown in Fig. 7.

In Fig. 7, we can see that the center frequency and the 10-dB bandwidth of the RF spectrum are nearly invariant when the optical carrier wavelength varies from 1530 nm to 1560 nm, indicating that the UWB generation has good tolerance to the optical carrier wavelength.

3.2. Generation and Investigation of Negative Monocycle Pulses

When the MZM is biased at the negative slope, counter-phase modulation occurs in the MZM, and an inverted RZ signal is obtained. When the MZM is biased at 0.77 V, the SOA is biased at 180 mA, and the optical wavelength is set at 1549.88 nm, the generated negative monocycle pulse and its RF spectrum are shown in Fig. 8.

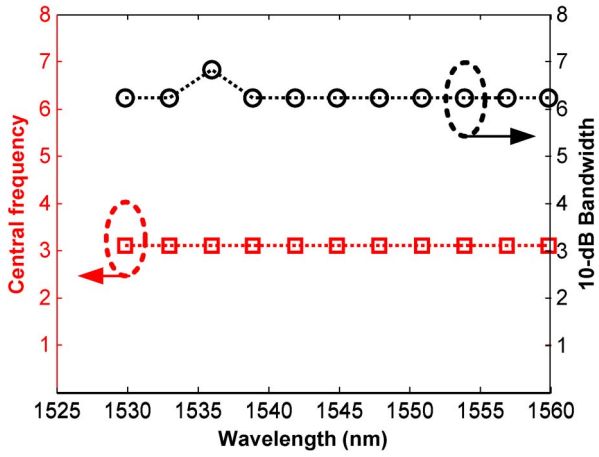

Fig. 7. Center frequencies (red dash rectangle line) and 10-dB bandwidths (black dash circle line) with different carrier wavelengths.

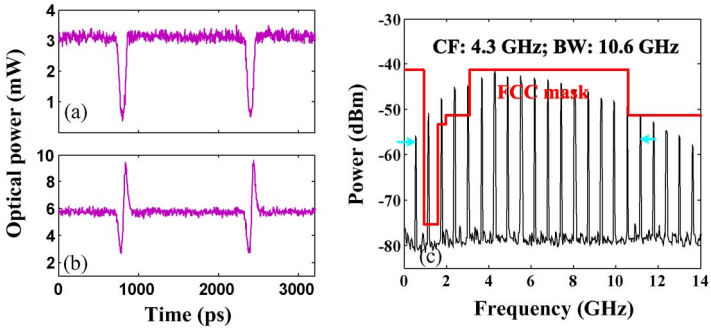

Fig. 8. (a) Intensity modulated optical pulse, (b) the generated optical waveform after SOA, and (c) its corresponding ESA.

The modulated optical signal is shown in Fig. 8(a). We can see that an inverted RZ signal is generated. The maximal optical power is 3.1 mW, and the minimal optical power is 0.5 mW. Then the inverted RZ signal is launched into the SOA. At the output of SOA, a negative monocycle pulse is obtained, as shown in Fig. 8(b). The upper and the lower amplitudes are 3.8 mW and 3.2 mW, and the upper and the lower FWHMs are 41 ps and 58 ps, respectively. Its RF spectrum is shown in Fig. 8(c). The center frequency and the 10-dB bandwidth are 4.3 GHz and 10.6 GHz (from 0.6 GHz to 11.2 GHz), respectively, with a fractional bandwidth of 247%. The mask infringement at the GPS band is also observed, and also can be improved by the UWB antenna, as stated in the earlier part.

The influence of bias current of SOA on generated negative UWB signals is shown in Fig. 9. When the bias current is 120 mA, the upper and the lower amplitudes are 1.9 mW and 1.6 mW and the upper and the lower FWHMs are 51 ps and 70 ps, respectively, as shown in Fig. 9(a). When the bias current is increased to 180 mA, the upper and the lower amplitudes are 3.2 mW and 2.5 mW, and the upper and the lower FWHMs are 40 ps and 59 ps, respectively, as shown in Fig. 9(b), with a larger amplitude and a smaller FWHM. When the bias current is further increased to 240 mA, the upper and the lower amplitudes are 3.8 mW and 3.2 mW, and the upper and the lower FWHMs are 37 ps and 52 ps, respectively, as shown in Fig. 9(c). By comparing Fig. 9(a)–(c), we can see that the symmetry of the monocycle pulse is also improved by increasing the bias current of SOA. When the bias current of SOA is increased, both the upper and the lower amplitudes are increased, and both the upper and the lower FWHMs are decreased. When the bias current is increased from 120 mA to 180 mA, the center frequency remains at 4.3 GHz, but the 10-dB bandwidth is increased from

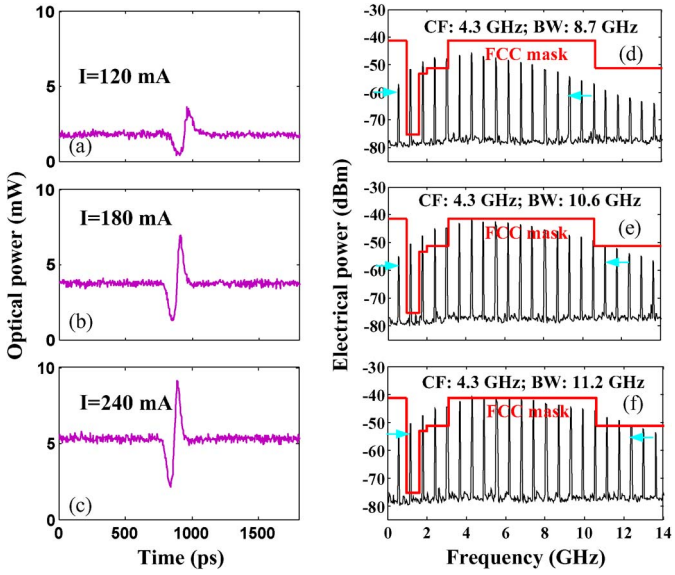

Fig. 9. (a)–(c) Generated negative monocycle pulses and (d)–(f) corresponding RF spectra when the SOA is biased at 120 mA, 180 mA, and 240 mA, respectively.

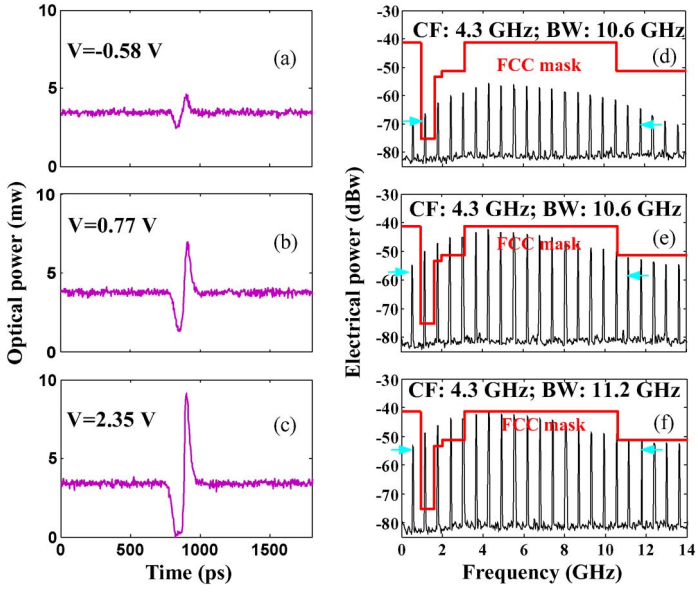

Fig. 10. (a)–(c) Generated monocycle pulses and (d)–(f) corresponding RF spectra when the MZM is biased at −0.58 V, −0.07 V, and 2.35 V.

8.7 GHz to 10.6 GHz, as shown in Fig. 9(d) and (e). However, when the bias current is increased to 240 mA, the 10-dB bandwidth is increased to 11.2 GHz, which exceeds the FCC regulation. Thus, a bias current of 180 mA is preferred.

Then the SOA is biased at 180 mA. The measured negative monocycle pulses and their corresponding RF spectra when the MZM is biased at different voltages are shown in Fig. 10. Fig. 10(a)–(c) show the generated negative monocycle waveforms. When the bias voltage is −0.58 V, the upper and the lower amplitudes are 1.2 mW and 1.1 mW, and the upper and the lower FWHMs are 41 ps and 47 ps, respectively, as shown in Fig. 10(a). When the bias voltage is increased to 0.77 V, the

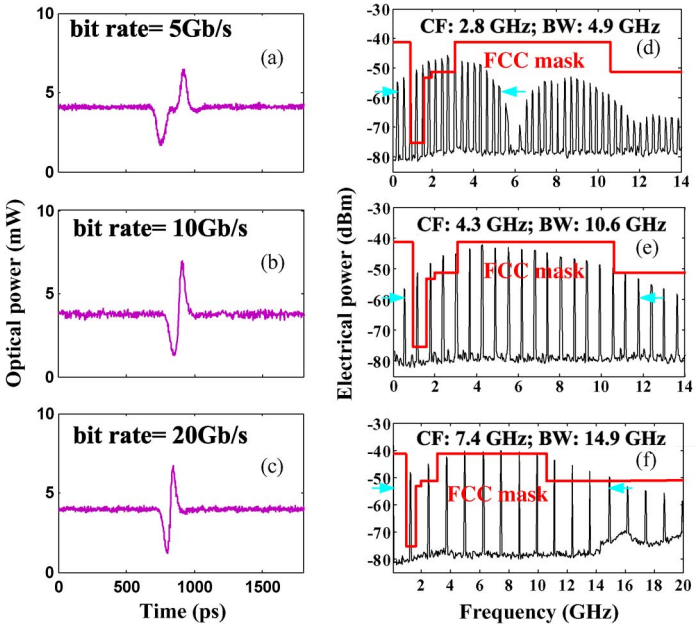

Fig. 11. (a)–(c) Generated optical waveforms and (d)–(f) their corresponding RF spectra, respectively.

upper and the lower amplitudes are both increased, as shown in Fig. 10(b). When the bias voltage is further increased to 2.35 V, the upper and the lower amplitudes are 4.9 mW and 3.2 mW, and the upper and the lower FWHMs are 37 ps and 71 ps, respectively. We can see that when the bias voltage is −0.58 V, the generated negative monocycle shows good symmetry, but the upper and the lower amplitudes are very small, leading to a low PSD, as shown in Fig. 10(d). The small amplitudes are caused by the nonlinear modulation in the MZM. When the bias voltage is increased to 0.77 V, the symmetry of the generated UWB monocycle pulse is not as good as that when the MZM is biased at 0.58 V, but the upper and the lower amplitudes of monocycle pulse are increased [as shown in Fig. 10(b)]. Correspondingly, the PSD is increased [as shown in Fig. 10(e)]. When the bias voltage is further increased to 2.35 V, the monocycle pulse shows distinct asymmetry, as shown in Fig. 10(c). The 10-dB bandwidth of its RF spectrum is 11.2 GHz, which is larger than the FCC definition, as shown in Fig. 10(f). In the experiment, a balanced bias voltage of the MZM is 0.77 V.

The generated optical waveforms and their RF spectra when the bit rate of the electrical signal is changed by tuning the BPG are shown in Fig. 11.

When the bit rate is 5 Gb/s, the generated negative monocycle pulse and its RF spectrum are shown in Fig. 11(a) and (d), respectively. The center frequency and the 10-dB bandwidth of the RF spectrum are 2.8 GHz and 4.9 GHz, respectively, as shown in Fig. 11(d). When the bit rate is 10 Gb/s, the generated negative monocycle pulse is shown in Fig. 11(b). Its RF spectrum is shown in Fig. 11(e). We can see that the center frequency and the 10-dB bandwidth are 4.3 GHz and 10.6 GHz, respectively. Fig. 11(c) and (f) show the generated negative monocycle pulse and its corresponding RF spectrum, respectively, when the bit rate is 20 Gb/s. In Fig. 11(f), we can see that the center frequency is 7.4 GHz and the 10-dB bandwidth is 14.9 GHz, which is larger than the FCC definition. The wider RF spectrum is caused by the narrower pulse width. The variations of center frequency and 10-dB bandwidth versus the optical wavelength are shown in Fig. 12.

In Fig. 12, we can see that the center frequency is nearly invariant when the optical wavelength is changed in the whole C-band, shown as the blue dashed square line in Fig. 12. The variation of the 10-dB bandwidth is as small as 0.6 GHz, shown as the black dashed circle line in Fig. 12. Therefore, the negative monocycle pulse also has good tolerance to the optical carrier.

By comparing Sections 3.1 and 3.2, it can be observed that the pulse width of the generated positive monocycle pulse is generally larger than that of the negative monocycle pulse, leading to a narrower

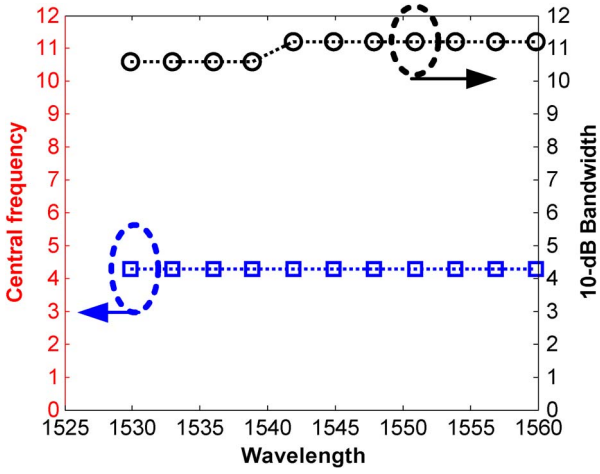

Fig. 12. Center frequencies (red dash rectangle line) and 10-dB bandwidths (black dash circle line) with different carrier wavelengths.

RF spectrum of the positive monocycle pulse. In the positive monocycle pulse, the center frequency is around 2.5 GHz and the 10-dB bandwidth is around 6.9 GHz. However, in the negative monocycle pulse, the center frequency is around 4.3 GHz, and the 10-dB bandwidth is around 10.6 GHz. When the bias current of SOA, the bias voltage of MZM, the bit rate of electrical signal, and the carrier wavelength are varied, respectively, the RF spectral difference still exists. The difference originates from the complementary carrier dynamic process. In the positive monocycle pulse generation, the carrier is depleted first and recovered second. While in the negative monocycle pulse generation, the carrier is recovered first and depleted second. In the SOA, the carrier behaves as fast depletion and slow recovery. Thus, difference occurs between the generated positive and the negative monocycle pulses.

It should be noted that the generated positive and negative monocycle pulses are frequency chirped because of carrier variation in this process. In the positive monocycle pulse generation, the carrier density is first decreased and then increased. Near the leading edge of the modulated optical pulses shown in Fig. 3(a), the carrier density of SOA is decreased because of carrier depletion, and the frequency chirp in the generated positive monocycle pulse is negative. However, near the trailing edge of the modulated optical pulse, the carrier density of SOA is increased because the carrier is recovering, leading to a positive frequency chirp [23]. On the other hand, in the negative monocycle pulse generation, the carrier density is first increased and then decreased. Near the leading edge of the modulated optical pulse shown in Fig. 8(a), the carrier density of SOA is increased because of carrier increment and the frequency chirp in generated negative monocycle pulse is positive. Near the trailing edge of the modulated optical pulse, the carrier density of SOA is decreased because of carrier depletion, leading to a negative frequency chirp. Therefore, the frequency chirps induced by carrier variation near the leading edge and the trailing edge of the optical pulse are opposite, and frequency chirps in the positive and the negative monocycle pulses are also opposite. It is worth noting that the chirp in generated monocycle pulses can be used to improve the symmetry of the monocycle pulse with the assistance of a detuned optical bandpass filter [20].

3.3. Discussions About UWB BPM

The scheme can be used to implement the BPM of UWB monocycle pulse. As discussed in Sections 3.1 and 3.2, the positive and the negative monocycle pulses can be generated when the MZM is biased at the positive and the negative slopes separately. An intuition thought of realizing monocycle BPM is to drive the bias port of MZM with electrical data encoded with a nonreturn-to-zero (NRZ) signal. However, for most commercial MZMs, the DC port is designed for a DC voltage

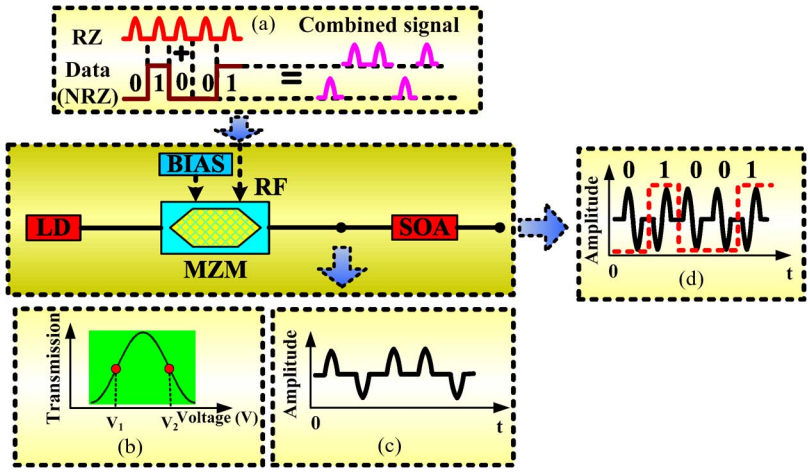

Fig. 13. Proposed method to realize UWB BPM using a commercial MZM.

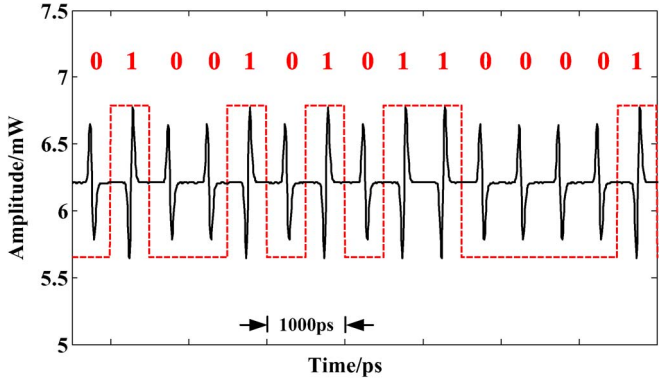

Fig. 14. Input NRZ signal (red dashed trace) and bi-phase modulated UWB monocycle pulse sequence (black solid trace).

and not for an RF signal with high frequency. Therefore, we propose another method to switch the bias voltage of the MZM. The principle is shown in Fig. 13.

In Fig. 13, the CW light is intensity modulated by the MZM, which is driven by a mixed electrical signal. The mixed signal is comprised of electrical data with NRZ format and an electrical sequence encoded with RZ format, as shown in Fig. 13(a). The mixing process is realized by using an RF power combiner. Here, the NRZ is encoded with a fixed pattern "01001." The NRZ signal is used to switch the bias point and the RZ signal is used to generate the monocycle pulse. Then, the mixed signal is applied to the RF port of the MZM. The RF port can be driven by an AC signal with high frequency. The modulation curve of MZM is shown in Fig. 13(b). V_1 and V_2 denote the two bias voltages that switched by the NRZ signal. At the output of MZM, an optical Gaussian sequence with opposite polarities is generated, as shown in Fig. 13(c). Then the optical sequence is injected into the SOA. After nonlinear amplification in SOA, bi-phase encoded monocycle pulses are generated, as shown in Fig. 13(d).

Because of hardware limitation, we carry out simulations about BPM of monocycle pulses using a photonic design automation tool called Virtual Photonics Inc. (VPI). In simulation, the half-wave voltage (V_π) is 5 V and the amplitude of "1" in the NRZ data is 3 V. The simulation result is shown in Fig. 14. The dashed trace represents the electrical NRZ signal and the solid trace represents the generated monocycle pulse sequence. The NRZ is encoded with the fixed pattern "010010101100001." We can see that the information encoded in the electrical NRZ signal is phase modulated onto the monocycle pulse. The negative monocycle pulse represents "1" and the

positive monocycle pulse represents "0." Thus, UWB BPM is realized. The unequal amplitudes of positive and negative monocycle pulses are caused by the gain saturation effect of the SOA.

4. Conclusion

We have proposed and experimentally demonstrated an approach to generating a pair of polarity-reversed monocycle pulses. Positive and negative monocycle pulses are generated when the MZM is biased at the positive and the negative slopes of the modulation curve, respectively. Both the RF spectra of generated polarity-reversed monocycle pulses comply with the FCC definition very well. The influences of the injection current of SOA, the bias voltage of MZM, the carrier wavelength and the pulse width on the monocycle pulse and the RF spectrum are experimentally studied. Experimental results show that the bias voltage of MZM, the bias current of SOA and pulse width of electrical signal can affect the generated monocycle pulse distinctively, but the influences of the optical carrier wavelength on monocycle pulse is tolerable, and the scheme can be implemented in the whole C-band. The symmetry of both the positive and negative monocycle pulses can be improved by increasing the bias current of SOA. Due to the character of fast depletion and slow recovery of the carrier in SOA, the pulse width of the positive monocycle pulse is wider than that of the negative monocycle pulse, leading to a narrower RF spectrum.

The BPM of UWB monocycle pulse is also feasible based on the scheme. In order to overcome the disadvantage that the NRZ signal cannot be applied to the bias port of a commercial MZM to switch the bias point, we propose to apply the NRZ signal to the RF port of the MZM. The simulation result shows that the UWB monocycle pulse can be bi-phase modulated by NRZ data.

References

[1] J. Yao, F. Zeng, and Q. Wang, "Photonic generation of ultrawideband signals," *IEEE J. Lightw. Technol.*, vol. 25, no. 11, pp. 3219–3235, Nov. 2007.

[2] M. Ghavami, L. B. Michael, and R. Kohno, *Ultra Wideband Signals and Systems in Communication Engineering*. West Sussex, U.K.: Wiley, 2004.

[3] M. G. D. Benedetto and G. Giancola, *Understanding Ultra Wide Band Radio Fundamentals*. Englewood Cliffs, NJ: Prentice-Hall, 2004.

[4] S. Pan and J. Yao, "A UWB over fiber system compatible with WDM-PON architecture," *IEEE Photon. Technol. Lett.*, vol. 22, no. 20, pp. 1500–1502, Oct. 2010.

[5] S. Pan and J. Yao, "Simultaneous provision of UWB and wired services in a WDM-PON network using a centralized light source," *IEEE Photon. J.*, vol. 2, no. 5, pp. 712–718, Oct. 2010.

[6] J. Yao, "Photonics for ultrawideband communications," *IEEE Microw. Mag.*, vol. 10, no. 4, pp. 82–95, Jun. 2009.

[7] X. Chen and S. Kiaei, "Monocycle shapes for ultra wide-band system," in *Proc. IEEE ISCAS*, Scottsdale, AZ, May 2002, vol. 1, pp. 597–600.

[8] F. Zeng and J. Yao, "Ultrawideband impulse radio signal generation using a high-speed electrooptic phase modulator and a fiber-Bragg-grating-based frequency discriminator," *IEEE Photon. Technol. Lett.*, vol. 18, no. 19, pp. 2062–2064, Oct. 2006.

[9] F. Zhang, S. Fu, J. Wu, N. Q. Ngo, K. Xu, Y. Li, X. Hong, P. Shum, and J. Lin, "UWB impulse radio transmitter using an electrooptic phase modulator together with a delay interferometer," *IEEE Photon. Technol. Lett.*, vol. 22, no. 20, pp. 1479–1481, Oct. 2010.

[10] J. Dong, X. Zhang, J. Xu, D. Huang, S. Fu, and P. Shum, "Ultrawideband monocycle generation using cross-phase modulation in a semiconductor optical amplifier," *Opt. Lett.*, vol. 32, no. 10, pp. 1223–1225, May 2007.

[11] S. Pan and J. Yao, "Switchable UWB pulse generation using a phase modulator and a reconfigurable asymmetric Mach–Zehnder interferometer," *Opt. Lett.*, vol. 34, no. 2, pp. 160–162, Jan. 2009.

[12] S. Wang, H. Chen, M. Xin, M. Chen, and S. Xie, "Optical ultra-wide-band pulse bipolar and shape modulation based on a symmetric PM–IM conversion architecture," *Opt. Lett.*, vol. 34, no. 20, pp. 3092–3094, Oct. 2009.

[13] J. Li, S. Fu, K. Xu, J. Wu, J. Lin, M. Tang, and P. Shum, "Photonic ultrawideband monocycle pulse generation using a single electro-optic modulator," *Opt. Lett.*, vol. 33, no. 3, pp. 288–290, Feb. 2008.

[14] M. Bolea, J. Mora, B. Ortega, and J. Capmany, "Optical UWB pulse generator using an N tap microwave photonic filter and phase inversion adaptable to different pulse modulation formats," *Opt. Exp.*, vol. 17, no. 7, pp. 5023–5032, Mar. 2009.

[15] J. Li, B. P. P. Kuo, and K. K. Y. Wong, "Ultra-wideband pulse generation based on cross-gain modulation in fiber optical parametric amplifier," *IEEE Photon. Technol. Lett.*, vol. 21, no. 4, pp. 212–214, Feb. 2009.

[16] S. Pan and J. Yao, "UWB-over-fiber communications: Modulation and transmission," *J. Lightw. Technol.*, vol. 28, no. 16, pp. 2445–2455, Aug. 2010.

[17] X. Yu, T. B. Gibbon, and I. T. Monroy, "Experimental demonstration of all-optical 781.25-Mb/s binary phase-coded UWB signal generation and transmission," *IEEE Photon. Technol. Lett.*, vol. 21, no. 17, pp. 1235–1237, Sep. 2009.

[18] S. Pan and J. Yao, "A photonic UWB generator reconfigurable for multiple modulation formats," *IEEE Photon. Technol. Lett.*, vol. 21, no. 19, pp. 1381–1383, Oct. 2009.
[19] X. Xu, E. Zhou, Y. Liang, T. Yuk, K. Lui, and K. Wong, "Power-efficient photonic BPSK coded ultrawideband signal generation," presented at the Proc. OFC/NFOEC, Los Angeles, CA, Mar. 2011, Paper OTuF5.
[20] J. Dong, X. Zhang, J. Xu, and D. Huang, "All-optical ultrawideband monocycle generation utilizing gain saturation of a dark return-to-zero signal in a semiconductor optical amplifier," *Opt. Lett.*, vol. 32, no. 15, pp. 2158–2160, Aug. 2007.
[21] X. Yu, T. B. Gibbon, M. Pawlik, S. Blaaberg, and I. T. Monroy, "A photonic ultra-wideband pulse generator based on relaxation oscillations of a semiconductor laser," *Opt. Exp.*, vol. 17, no. 12, pp. 9680–9687, Jun. 2009.
[22] J. Capmany, D. Pastor, A. Martinez, B. Ortega, and S. Sales, "Microwave photonic filters with negative coefficients based on phase inversion in an electro-optic modulator," *Opt. Lett.*, vol. 28, no. 16, pp. 1415–1417, Aug. 2003.
[23] J. Dong, X. Zhang, S. Fu, J. Xu, P. Shum, and D. Huang, "Ultrafast all-optical signal processing based on single semiconductor optical amplifier and optical filtering," *IEEE J. Sel. Topics Quantum Electron.*, vol. 14, no. 3, pp. 770–778, May/Jun. 2008.